Journal of the Serbian Society for Computational Mechanics / Vol. 18 / No. 1, 2024 / pp 79-93 / original paper
(10.24874/jsscm.2024.18.01.06)

EFFECTS OF GAS RADIATION AND ACCELERATED FLOW ON SOLAR HEATER PERFORMANCE

Seyed Abdolreza Gandjalikhan Nassab [0000-0003-0783-3155]

Mechanical Engineering Department, School of Engineering, Shahid Bahonar University of Kerman, Kerman, Iran
e-mail: ganj110@uk.ac.ir

Abstract

In this paper, the performance enhancement of solar gas heaters is evaluated by taking the advantage of both radiating gas effect and using converged ducts with the accelerated flow. The analyzed solar gas heater includes the glass cover, air gap, absorber, gas channel, bottom plate, and insulation. The inclined position of the bottom plate relative to the absorber provides a converged shape for the duct of the heater. For the free convection airflow inside the air gap and forced convection gas flow in the heater's duct, the CFD-based numerical simulations are carried out by the finite element method via the COMSOL software. Numerical results reveal the positive effect of gas radiation with the fact that in the downstream side of gas flow with a small convection coefficient, the gas accelerated flow with extra turbulence breaks down the thermal boundary layer and augments the convection heat transfer rate. For the studied test cases, 18% and 8% increases in thermal efficiency are observed due to the gas radiation and inclined position of the bottom plate, respectively. Consistency between the obtained numerical findings and experimental data shows the accuracy of the applied numerical method.

Keywords: gas radiation, converged duct, solar gas heater, efficiency.

1. Introduction

The performance enhancement in solar air heaters (SAHs) is the subject of a huge number of research papers during the past 30 years and many techniques have been suggested by scientists up to now. A review of different methods for increasing the efficiency of SAHs was reported by Ahirwar (2024). Most of the suggested techniques deal with the convection augmentation by increasing the surface and coefficient of heat transfer by employing fins (Manca 2011), artificially roughened surfaces (Singh 2011), vortex generators (Sheikhnejad 2021), porous segments (Naphon 2005), Wavy channels (Singh 2022), perforated absorber plates with different geometries (Sreyas 2021) and jet impingement method (Alomar 2022). Recently, Forouzan Nia (2020) examined the effect of gas radiation and the use of radiating gas instead of air as the working gas inside a closed loop including the solar gas heater and an extra heat exchanger, and up to 10% increase in thermal efficiency was reported. Also, changing the rectangular shape of the air duct into the converged configuration was studied by the Gandjalikhan Nassab (2023) and Gandjalikhan Nassab (2024) and it was found as a suitable improvement technique. In the present paper, the combined effect of gas radiation and the use of converged duct in the construction of solar gas heater (SGH) is studied using the Computational Fluid Dynamics (CFD) technique. Since the gas flows under the absorber plate (Fig. 1), an air gap is considered above the heater absorber and both free and forced convection flows take place inside the SGH. In the analysis, the governing equations for these two turbulent flows along with the conduction equation for the solid parts are solved simultaneously utilizing the finite element method (FEM). Several test cases with different values of the converging ratio and gas optical thickness are analyzed and the obtained numerical data are depicted in terms of isotherm plots and velocity and pressure distributions in different parts of the proposed SGH.

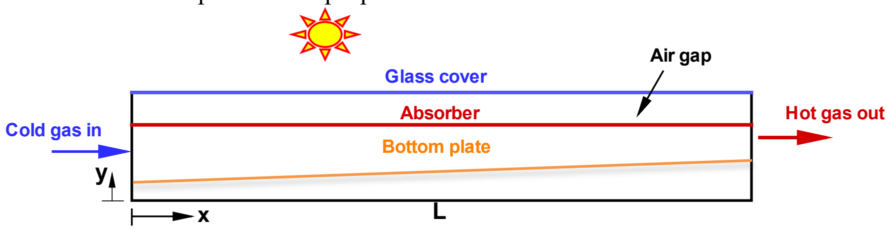

Fig. 1. Schematic of the proposed SGH, L=1 m, b= 4 cm

2. Computational model

Fig. 1 illustrates a schematic of the analyzed SGH. The dimensions of the heater with the values of some physical properties and geometrical parameters are given in Tables 1 and 2. In the design of SGH, the bottom plate has the ability to rotate around its central point for providing the converged shape for the duct of heater. In the base model with zero bottom plate inclination angle, (CR=A_{in}/A_{out}=1), the height of the heater's duct is considered equal to b=4 cm, while in the test cases with the converged duct, the value of converging ratio, CR, can be computed by:

$$CR = \frac{A_{in}}{A_{out}} = \frac{b + 0.5L\tan(\theta)}{b - 0.5L\tan(\theta)} \tag{1}$$

where θ is the bottom plate inclination angle with the horizontal x-axis due to the rotation of this element around its central point. Gas flow with the ambient temperature and fully developed velocity profile enters into the heater and inside the duct and the velocity increases due to the converged channel. Different values of gas flow rates including $\dot{m} = 0.01$ to 0.04 kg/s, all in the range of turbulent flow are considered in simulations. The working gas has the same values of density, thermal conductivity and heat capacity as air, except for its radiative absorption coefficient. For the free convection flow inside the air gap, the value of Rayleigh number, $Ra = g\beta\Delta T\, a^3 / \nu\alpha$ becomes greater than $Ra_c = 5 \times 10^4$ denotes the turbulent regime (Incropera 2002).

In the numerical simulation, it is assumed that, from the total incident solar irradiation, a small part equal to $\alpha_g . q_{sun}$ is absorbed by the glass cover and is considered as a source term in the conduction equation for this element and a major part of the transmitted radiation, $\tau_g . \alpha_{abs} . q_{sun}$ absorbs by the black-painted absorber plate. The top and bottom boundary surfaces are in heat transfer with the surrounding by combined free convection and surface radiation with the equivalent heat transfer coefficient of $h_{eq} = h_{conv} + h_{rad}$, such that the other side boundary surfaces are adiabatic (Singh (2017)). In numerical simulations, three different values of the inclination angle θ, including the horizontal case for the base model, are considered. According to Eq. 1, the convergence ratio CR=A_{in}/A_{out}, varies with the inclination angle whose values for the three studied test cases are given in Table. 3.

Physical properties	Absorber	Insulation	Bottom plate	Glass cover
Thermal conductivity [W/m.K]	402	0.036	402	0.8
Surface emissivity	0.97	_	0.97	0.97
Reflectivity	0.03	_	0.03	0.02
Transmissivity	0	0	0	0.95

Table 1. Material properties

Parameter	a	b	L	$\boldsymbol{\delta_g}$	$\boldsymbol{\delta_{abs}}$	$\boldsymbol{\delta_{bp}}$	$\boldsymbol{\delta_{ins}}$
Value (mm)	20	40	1000	4	2	2	50

Table 2. Values of the geometrical parameters.

$\boldsymbol{\theta}$ (Degree)	Converging ratio
0	1
1.5	1.97
3	4.8

Table 3. Values of converging ratio at different inclined angle

3. Governing equations

The conservative form of the equation governs the applied numerical model and can be written as follows:

$$\nabla_{.}(\rho\vec{U}\varphi) = \nabla_{.}(\Gamma_{\varphi}\nabla\varphi) + S_{\varphi} \tag{2}$$

where φ as each of the dependent variables stands for velocity components, temperature, turbulent dissipation rate, and kinetic energy, ρ is the density, $\vec{U}$ the vector of velocity, while Γ_{φ} and S_{φ} are the source term and diffusion coefficient, respectively. For each dependent variable, the parameters Γ_{φ} and S_{φ} are different and their particular expressions are given by Launder (1974). These equations for steady-state incompressible turbulent free and forced convection flows are solved by the standard $k-\varepsilon$ model and the RANS method applied by Sigth (2019), with appropriate boundary conditions demonstrated in Fig. 2. In the analysis of radiating gas flow, the radiative source term $\nabla.\, q_{rad}$ due to the gas radiation effect should be considered in the energy equation which can be computed as in Modest (2003):

$$\nabla_{.}\overrightarrow{q_r} = \sigma_a(4\pi I_b(\vec{r}) - \int_{4\pi} I(\vec{r},\vec{s})d\Omega) \tag{3}$$

The relation between the radiant intensity $I(\vec{r},\vec{s})$ with the gas temperature according to the radiative transfer equation (RTE) for non-scattering medium is as given by Modest (2003):

$$(\vec{s}.\nabla)I(\vec{r},\vec{s}) = -\sigma_a I(\vec{r},\vec{s}) + \sigma_a I_b(\vec{r}) + \frac{\sigma_s}{4\pi}\int_{4\pi} I(\vec{r},\vec{s})\varphi(\vec{s},\vec{s})d\Omega) \tag{4}$$

In numerical solution of the RTE, the following boundary condition on the boundary surfaces is applied:

$$I(\vec{r}_w,\vec{s}) = \varepsilon_w I_b(\vec{r}_w) + \frac{1-\varepsilon_w}{\pi}\int_{\vec{n}_w.\vec{s}<0} I(\vec{r}_w,\vec{s})\left|\vec{n}_w.\vec{s}'\right| d\Omega' \quad \vec{n}_w.\vec{s} > 0 \tag{5}$$

In the paper by Foruzan Nia (2020), the details of numerical model in solving RTE with the discrete ordinate method were described. For space-saving, the readers are referred to that reference about the solution of radiative transfer equation and also the boundary conditions applied in the numerical model. In the present study, the working gas is assumed as an absorbing-emitting and non-scattering participating medium ($\sigma_s = 0$), such that the value of optical thickness which is defined as $\tau = \sigma_a.b$ shows the ability of gas flow in radiation heat transfer. In all simulations, for having different optical thicknesses, the value of b is kept constant and various values of the gas absorption coefficient, σ_a are considered for having different optical thicknesses, including $\sigma_a = 0$, for the non-radiating working gas.

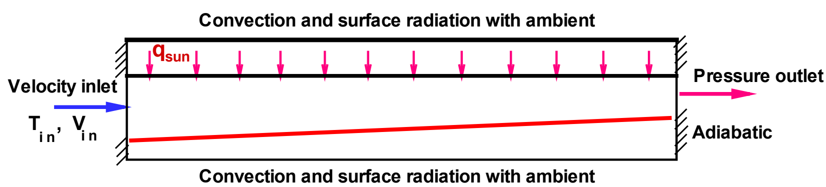

Fig. 2 Applied boundary conditions

3.1 Mesh study

To find the grid-independent solution, the value of the average Nusselt number ($\overline{Nu} = \bar{h}b/k$) on the heated absorber surface was checked against the mesh sizes as tabulated in Table 4. Based on the obtained results, the discretized computational domain with 21060 nodes shown in Fig. 3 is considered as the optimum grid at which the percentage of error becomes less than 1%. It should be noted that the amount of error is calculated as the percentage of Nusselt number variation along two susequent grid sizes.

Number of nodes	9720	13230	17010	21060	25470
$\overline{Nu}$	9.46	10	10.29	10.39	10.42
Percent of error	-	5.7	2.9	0.97	0.3

Table 4. Average Nusselt number at different grid sizes

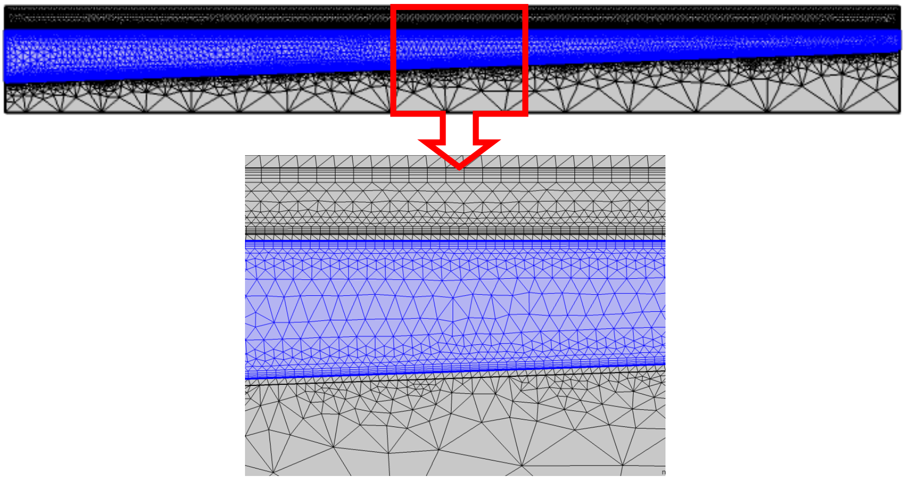

Fig. 3. Discretized computational plane ($\theta = 3^0$)

4. Validation

The present paper includes both gas radiation computation by solving the RTE and the velocity, pressure and temperature computations from the Navier-stokes and energy equations for forced convective airflow by the CFD technique. Thereby, the numerical findings are compared with the those found by Foruzan Nia (2020) for verifying the solution of radiative transfer equation and then by experimental data by Ramani (2010) for flow simulation. The variation of temperature along the y-axis across the SGH at axial sections x=L/4 and x=L are plotted in Fig. 4 for the gas optical thickness of 2. As seen, insulation temperature increases with a linear trend up to the absorber where the highest maximum temperature takes place. Inside the gas flow, the positive influence of gas radiation in heating the convection flow in clearly observed. However, a close agreement with the maximum error of 1.5% exists between the present numerical results and those obtained by Foruzan Nia (2020).

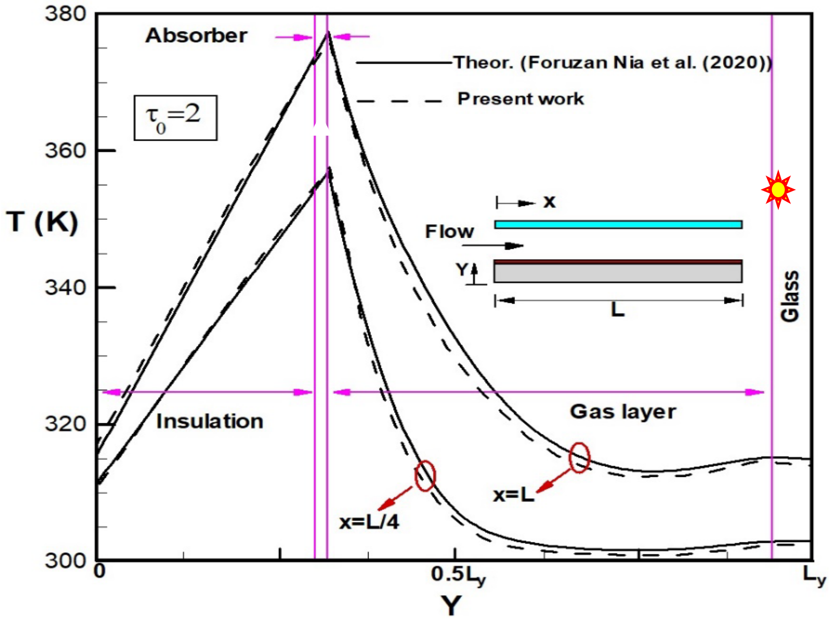

Fig. 4. Comparison of the present numerical results with the findings by Foruzan et al.

The second validation is about the convective flow simulation of a double-pass SAH which was studied by Ramani (2010). This air heater is analyzed here by the FEM and the flow and thermal behavior of SAH is obtained from the numerical findings. The simulated SAH is a buble-pass type that contains the glass cover, upper and lower air ducts, absorber plate and insulation, whose geometrical details were given by Ramani (2010). By the obtained air outlet temperature, the value of thermal efficiency of the analyzed SAH is calculated according to the following relation:

$$eta_t = \frac{\dot{m}c_p(T_{mout} - T_{in})}{q_{sun}A} \tag{6}$$

The variation of thermal efficiency with the solar heat flux is drawn in Fig. 5. Experimental and numerical results presented in this figure show that the thermal efficiency of SAH increases with the increase of solar incoming radiation. The maximum value of deviation in the predicted thermal efficiencies is about ±6%, indicating a good consistency.

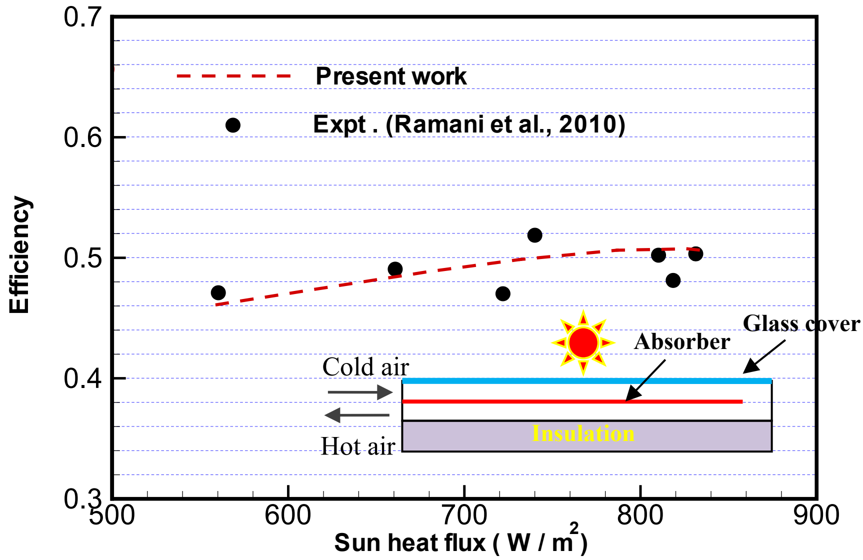

Fig. 5. Variation of thermal efficiency with solar irradiation

5. Results

In this part of the paper, the numerical findings are reported for several test cases to examine both the effects of gas radiation and accelerated convection gas flow on the performance of the proposed SGH. In the following results, the values of solar irradiation and the gas mass flow rate are kept constant and equal to 1000 W/m^2 and 0.01 kg/s, respectively. All numerical simulations are carried out at three different bottom plate inclined angles $\theta = 0^0, 1.5^0$ and 3^0 corresponding to CR=1, 1.97, and 4.8 and four different values of the gas optical thickness $\tau = 0.0.4, 0.2$ and 0.4. The effects of gas radiation and the inclined angle on the thermal behavior of SGH are studied in Fig. 6 by plotting the temperature fields at different values of the gas optical thickness and the inclination angle including the non-radiating gas ($\tau = 0$), and the horizontal bottom plate ($\theta = 0^0$) as the base model. This figure shows how the gas flow receives thermal energy from the heated surface by both convection and radiation heat transfer. In all test cases, the highest temperature belongs to the absorber and the air gap above this element. Comparison between the isotherm plots at different conditions can show the gas radiation and the converged duct effects on the performance of SGH. As seen, the thermal energy penetration dept from the heated absorber into the gas flow increases as the optical thickness gets higher values, such that this behavior is enhanced for the cases with more inclined angles. One can notice that there is a considerable decrease in the air gap and glass cover temperature in the case of using radiating gas. This behavior leads to a lower rate of energy loss to the environment. The minimum outlet gas temperature belongs to the base model with non-radiating gas and the maximum one to the test case with $\tau = 0.4$ and $\theta = 3^0$. This behavior reveals the positive effects of gas radiation with the converged duct on heat transfer augmentation.

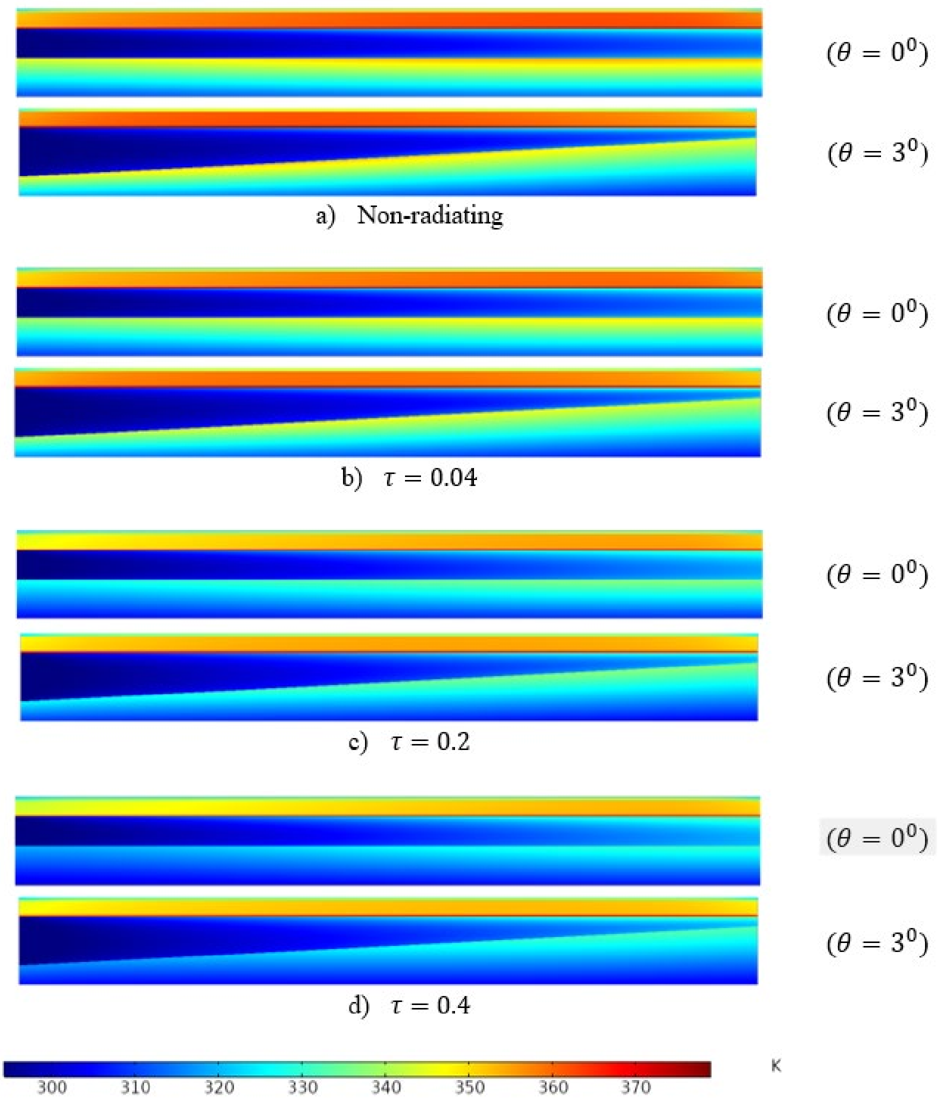

Fig. 6. Isotherm plots at different optical thickness for $\theta = 0^0, 3^0$

To study more about the effect of gas radiation, the variations of gas bulk temperature along the base model $(\theta = 0^0)$ are plotted in Fig. 7. An almost linear increasing trend of the gas temperature along the SGH is seen for each case, such that the minimum gas outlet temperature belongs to the non-radiating gas and the maximum one for the strong radiating gas $(\tau = 0.4)$, with more than $7\,^0$C temperature difference.

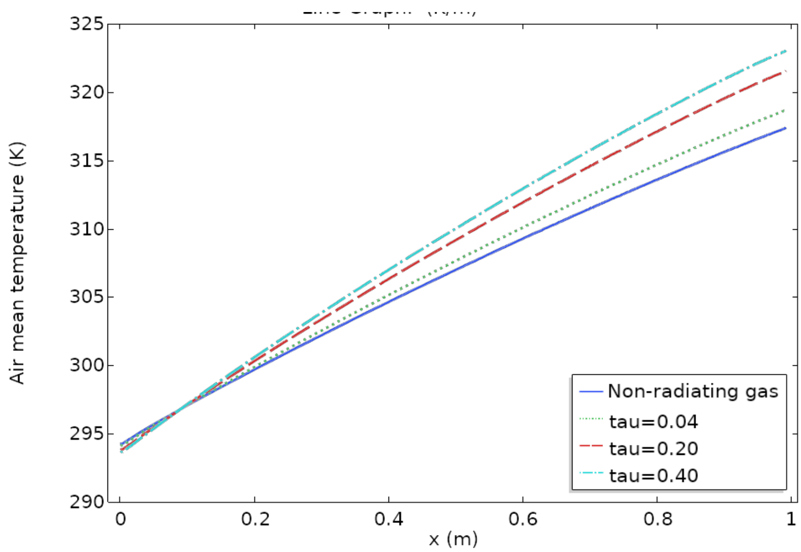

Fig. 7. Variation of gas bulk temperature along the heater, $\theta = 0^0$

One of the undesired phenomena due to using converged ducts in the construction of SGHs is the increase in pressure drop. To verify this fact, the gas pressure fields for the straight and converged ducts are depicted in Fig. 8. This figure shows that the amount of the studied parameter for the converged duct with $\theta = 3^0$ is about 17 times the one in the base model. It might be a serious criterion in designing the converged ducts, but due to a very small pressure drop for the usual mass flow rate, say $\dot{m} = 0.01\ kg/s$, the increase in the pumping power ($\dot{m}\Delta p/\rho$) for the proposed SGH could not be an important limitation.

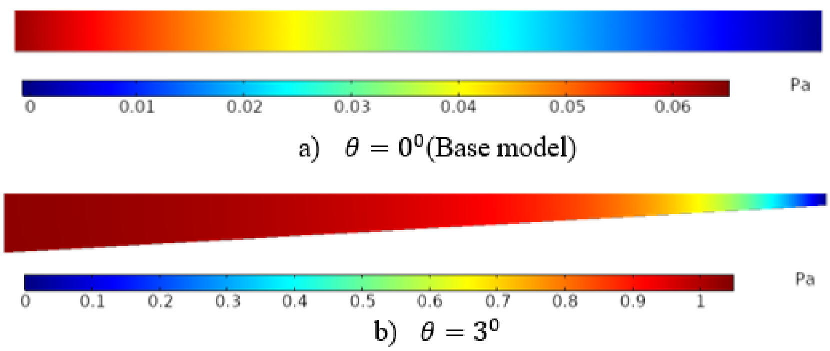

Fig. 8. Isobar plots

To predict the thermal characteristics of SGH, the temperature variations along the absorber plate at different values of the bottom plate inclined angle and gas optical thickness are plotted in Fig. 9. As seen, in the cases of using radiating working gas in which the gas flow receives thermal energy by both convection and radiation heat transfer, the absorber temperature decreases by the increase of gas optical thickness. One more important aspect observed from Fig. 9 is the different trends for the absorber temperature variation along this element, such that in the case of accelerated flow $\theta = 3$ degrees, after a local maximum temperature at the upstream side, the absorber temperature decreases along the flow direction due to growth of convection coefficient.

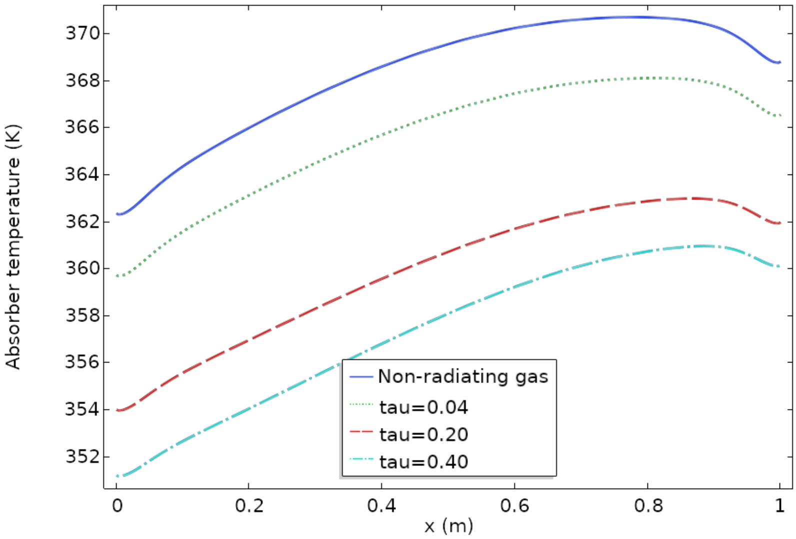

(a)

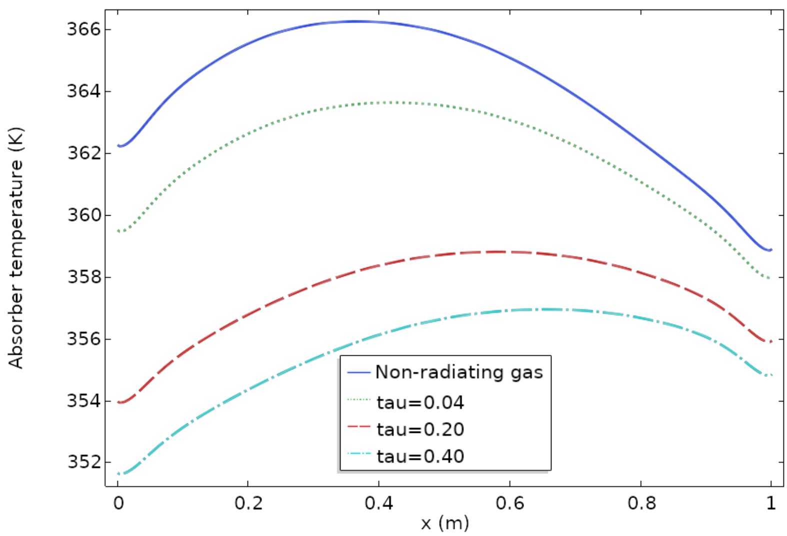

(b)

Fig. 9. Absorber temperature distribution (a) $\theta = 0^0$ $b)$ $\theta = 3^0$

The effects of gas radiation and the inclined angle of bottom plate on the glass temperature distribution are shown in Fig. 10. High-temperature gradients are seen near the two endpoints with minimum temperatures and more uniform distribution at the central zone. This figure reveals the positive gas radiation effect on the performance of SGH such that the maximum value of glass temperature happens for the base model with non-radiating gas flow. Comparison between the curves plotted in Fig. 10-a and b reveals about 4 C decreases in the average glass temperature due to the usage of a converged duct. This behavior has an important role in performance improvement because the major part of heat loss takes place via the glass cover.

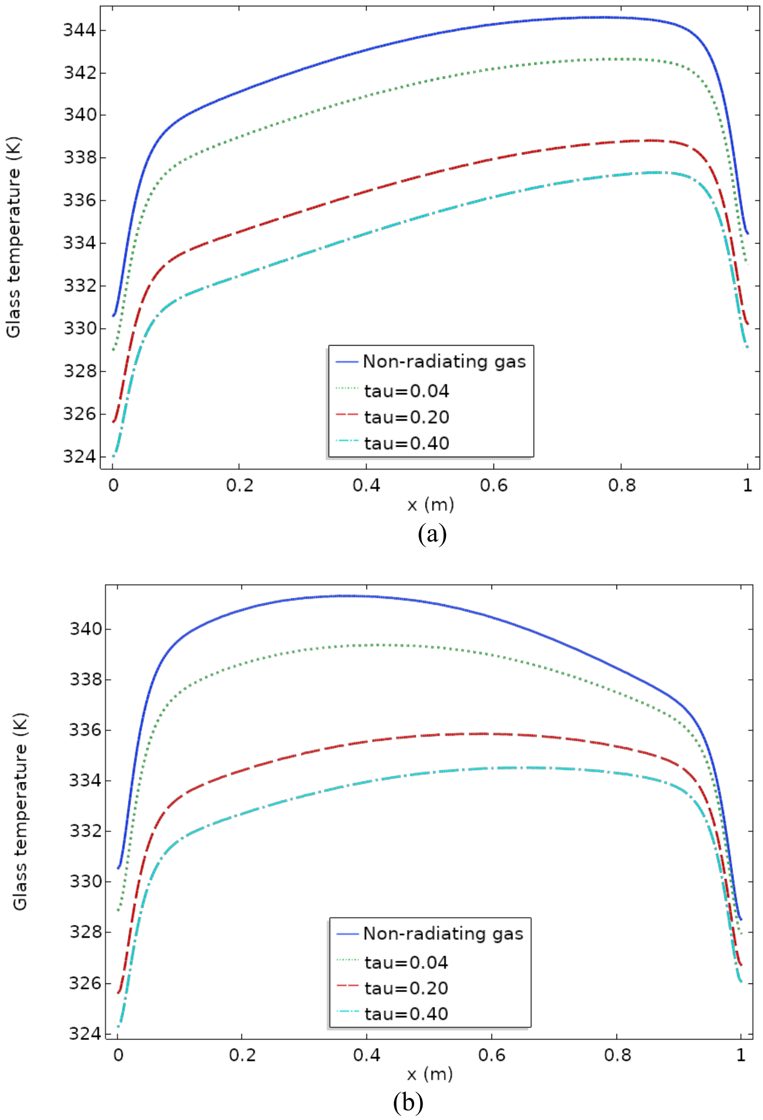

Fig. 10. Glass temperature distributions at different gas optical thickness and bottom plate inclined angle $a)\ \theta = 0^0\ b)\ \theta = 3^0$

The temperature variations across the SGH for different values of the gas optical thickness and inclined angle at two axial sections x=L/3 and 2L/3 are drawn in Fig. 11. Temperature distribution inside the solid element and also in the air gap has a linear trend. It is seen that the maximum gas temperatures take place adjacent to the absorber and bottom plate and the convective gas flow receives thermal energy from these two heated surfaces. This process enhances at high optical thickness, especially for the converged duct with $\theta = 3$.

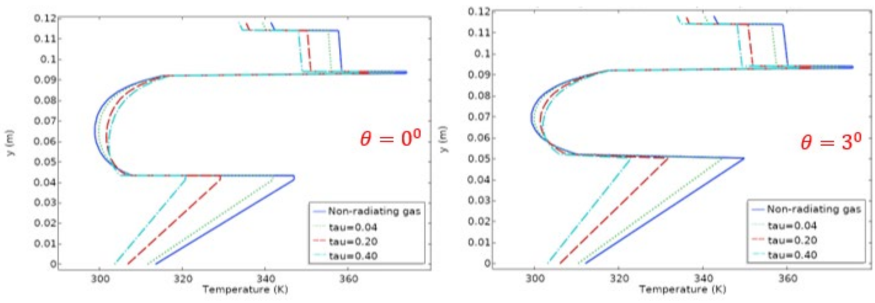

(a)

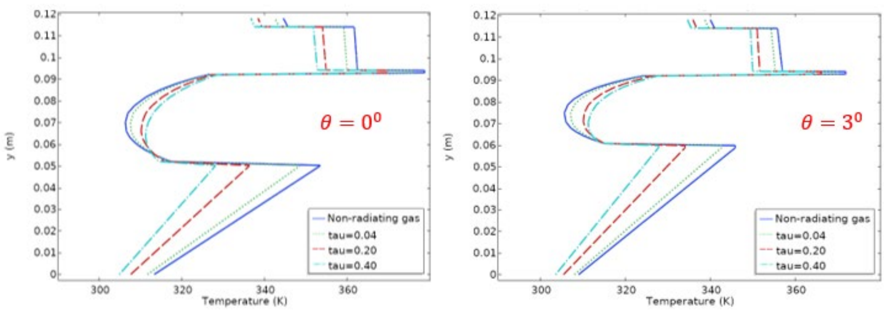

(b)

Fig. 11. Temperature variation in y-direction a) x=L/3 b) x=2L/3

In Fig. 12, the variations of thermal efficiency with the gas optical thickness at three different values of the inclined angle are plotted. This figure reveals the increase of thermal efficiency as the gas optical thickness and inclination angle get higher values. Compared to the base model with non-radiating gas, the percentages of efficiency increase about 8% and 18% can be computed due to the converged duct and gas radiation effect for the test cases, respectively.

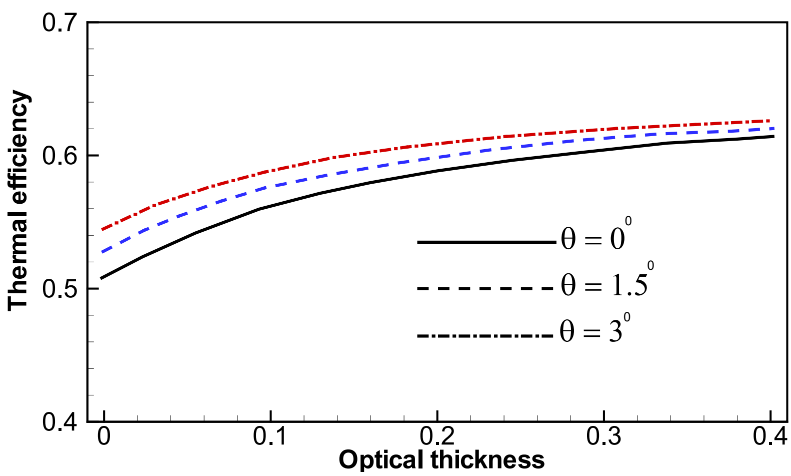

Fig. 12. Thermal efficiency vs gas optical thickness at different bottom plate inclined angle

6. Conclusion

This study was dedicated to the examination of the roles of converged air ducts and gas radiation effect in the construction of SGHs for higher thermal efficiency. Along a CFD-based numerical analysis, the set of governing equations, including continuity, momentum, and energy for steady 2-D turbulent forced and free convection flows and the Laplace equations for solid elements has been solved by the finite element method. Through the numerical findings, the converged duct and gas radiation effect proved well their potentials in heat transfer augmentation. In this regard, the highest percentages of efficiency increase of about 8% and 18% have been computed due to the inclined bottom plate (converged duct) and using radiating working gas for the proposed SGH compared to the base model.

Nomenclature

A	Area	$\boldsymbol{\tau_g}$	Glass transmissivity
a	Air gap thickness (m)	β	Volumetric thermal expansion (1/K)
b	Height of the heater duct (m)	μ	Fluid Viscosity (Pa.s)
CR	Converging ratio	ρ	Fluid density (kg/m ^{3})
$\boldsymbol{C_p}$	Gas specific heat (kJ/kg K)	θ	Bottom plate inclined angle
h	Convection coefficient (W/m^{2}K)	υ	Dynamic viscosity (m^2/s)
I	Radiant intensity ($W / m^2 .st$)	σ_a	Absorption coefficient (1/m)
k	Thermal conductivity (Wm^{-1}K^{-1})	σ_s	Scattering coefficient (1/m)
L	Length of heater (mm)	τ	Optical thickness
Nu	Nusselt number	Ω	Solid angle (st)
$\vec{\boldsymbol{n}}$	Normal vector (m)	δ	Thickness (m)
p	Pressure (Pa)	**Subscript**	
q	Heat flux (W/m^2)	abs	Absorber
$\vec{\boldsymbol{r}}$	Position vector (m)	amb	Ambient
Re	Reynolds number =$\rho\overline{V_{in}}b/\mu$	b	Black body
s	Direction	bp	Bottom plate
T	Temperature (K)	eq	Equivalent
V	Velocity vector (m/s)	g	Glass
(x, y)	Coordinates (m)	in	Inlet
Greek symbols		ins	Insulation
$\boldsymbol{\alpha_g}$	Glass absorptivity	out	Outlet
$\boldsymbol{\rho_g}$	Glass reflectivity	w	wall

References:

Ahiwar B K, Kumar A (2024). Review on different techniques to enhance the thermal performance of solar air heaters, *International Journal of Heat and Mass transfer*, 220, 124979.

Alomar O R, Maher Abd H, Mohamed Salih MM (2022). Efficiency enhancement of solar air heater collector by modifying jet impingement with v-corrugated absorber plate, *Journal of Energy Storage*, 55, Part B, 105535.

Foruzan Nia M, Gandjalikhan Nassab S A, Ansari A B (2020). Numerical simulation of flow and thermal behavior of radiating gas flow in plane solar heaters, *J. Therm. Sci. Eng. Appl*. 12, 031008.

Gandjalikhan Nassab S A (2023). Efficient design of converged ducts in solar air heaters for higher performance, *Heat Mass Transfer*, 59 (3), 363-375.

Gandjalikhan Nassab S A (2024). Three-dimensional CFD analysis of solar air heaters for improving thermal performance using the converged air ducts, *International Journal of Green Energy*, 21 (1), 43-53.

Incropera F P, Dewitt D P (2002). Introduction to Heat Transfer, Forth Edition,Wiley New York.

Launder B E, Spalding D B (1974). The numerical computation of turbulent flows, *Computer Methods in Applied Mechanics and Engineering*, 3(2), 269-289.

Manca O, Nardini S, Ricci D (2011). Numerical study of air forced convection in a channel provided with inclined ribs. ASME, International Heat Transfer Conference, 861-870.

Modest M (2003). *Radiative Heat Transfer*, 2nd ed., Academic Press.

Naphon P (2005). Effect of porous media on the performance of the double-pass flat plate solar air heater, *International Communication in Heat and Mass Transfer*, 32, 140-150.

Ramani B M, Gupta A, Kumar R (2010). Performance of a double pass solar air collector, *Solar Energy*, 84, 1929-1937.

Sheikhnejad Y, Gandjalikhan Nassab S A (2021). Enhancement of solar chimney performance by passive vortex generator, *Renewable Energy*, 169, 437-450.

Singh S, Chander S, Saini J S (2011). Heat transfer and friction factor correlations of solar air heater ducts artificially roughened with discrete V-down ribs, *Energy* 36 (8), 5053–5064.

Singh S (2022). Utilizing fractional porous interface for high thermal performance of serpentine wavy channel solar air heater, *Applied Thermal Engineering*, 205, 118044.

Singh A P, Akshayveer Kumar A, Singh O P (2019). Designs for high flow natural convection solar air Heaters, *Solar Energy* 193, 724-737

Singh S (2017). Performance evaluation of a novel solar air heater with arched absorber plate, *Renew. Energy*, 114, 879–886.

Sreya P, Shetty N, Madhwesh K, Vasudeva K (2021). Numerical analysis of a solar air heater with circular perforated absorber plate, *Solar Energy*, 215, 416-433.